Inviscid Axisymmetric Jet Impingement with Recirculating Stagnation Regions

A. Rubel*
Grumman Aerospace Corporation, Bethpage, New York

Numerical solutions for the normal impingement of inviscid axisymmetric jets with energy deficient cores reveal three distinct classes of behavior: 1) a small defect regime where the flow structure is unchanged from the zero defect case, 2) a moderate defect regime where stagnation bubbles first appear and grow with increased defect, and 3) a strong defect regime, where no solutions have been found. The recirculation zone model presumes that vorticity over radius is constant and continuous across the dividing stream surface. A local analytic solution to the governing partial differential equation for the stagnation bubble is consistent with the computational results.

Introduction

A PREVIOUS study[1] has demonstrated that the impact region of a jet impingement flowfield is dominated by inertia and pressure forces so that an inviscid, rotational flow model describes its basic features. This approach has successfully treated incompressible jets with velocities that monotonically decay from their centerline peak values. There is, however, another class of jet impingement problems where the central core exhibits a reduced total pressure. For example, certain fan jets considered for VTOL application have exhausts that are characterized by such profiles.[2] Furthermore, the impingement of underexpanded axisymmetric jets is subject to similar defects induced by centerline normal shock losses prior to impact. Observations of stagnation bubbles in such flows have been noted by several investigators (e.g., Donaldson and Snedeker,[3] Kalghatgi and Hunt,[4] and Lamont and Hunt[5]).

It is the purpose of this work to show that the inviscid, rotational flow model applied to the impingement of an axisymmetric jet with centerline total pressure defect can produce stagnation region recirculation zones. The appearance of recirculation zones in the context of the inviscid, rotational flow approximation is not unusual. Bossel[6] has computed a free circulating bubble induced by an adverse pressure gradient developed in a decaying swirl field. More recently, Hafez and Lovell[7] have calculated shock-induced separation regions in transonic flow situations. An analytic solution for an axisymmetric recirculating region is given by Hill's spherical vortex.[8,9] It is found here that this solution belongs to a wider class of axisymmetric bubbles and that within this class is a category that represents the stagnation bubbles detected by the numerical computations.

Formulation

Consider the normal impingement of an axisymmetric jet with a velocity defect, δw, at its axis (Fig. 1). A cylindrical (x,z) coordinate is used where x is in the direction normal to the jet centerline and z is directed along the centerline with origin at the impingement surface. In this formulation all velocities are normalized with respect to the jet maximum velocity located at a distance x_m from the axis. Lengths are scaled by the velocity half width. For inviscid, incompressible flow the governing equation is[1]

$$\frac{\partial^2\psi}{\partial z^2} + x\frac{\partial}{\partial x}\left(\frac{1}{x}\frac{\partial\psi}{\partial x}\right) = x^2\Omega(\psi) \tag{1}$$

where ψ is the stream function defined by

$$\partial\psi/\partial x = -xw, \qquad \partial\psi/\partial z = xu \tag{2}$$

and u, w are the velocities in the x, z directions, respectively. The vorticity function, $\Omega(\psi)$ is defined in terms of the vorticity ω, so that

$$\Omega(\psi) \equiv \frac{\omega}{x} \equiv \frac{1}{x}\left(\frac{\partial u}{\partial z} - \frac{\partial w}{\partial x}\right) \tag{3}$$

and it is "frozen" (i.e., constant) on inviscid streamlines. Therefore, the jet velocity profile determines $\Omega(\psi)$ throughout the flowfield except for regions of recirculation. In these regions the condition developed by Batchelor,[10] i.e., $\Omega(\psi) = \text{const}$, is utilized and the vorticity function is taken to

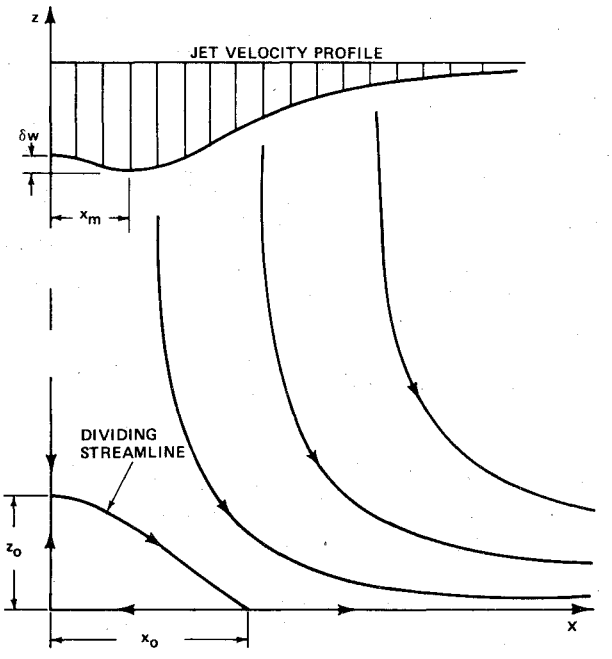

Fig. 1 Schematic of the jet impingement problem.

Presented as Paper 82-0297 at the AIAA 20th Aerospace Sciences Meeting, Orlando, Fla., Jan. 11-14, 1982; submitted Jan. 21, 1982; revision received June 19, 1982.

*Head, Theoretical Aerodynamics Laboratory, R&D Center. Member AIAA.

be continuous across the dividing streamline so that

$$\Omega(\psi) \equiv \Omega(0); \quad \psi \leq 0 \tag{4}$$

It is understood that prescription of the vorticity function within the recirculation zone is arbitrary, but, for the purposes of this work, it would appear that Eq. (4) is a logical choice. The system is closed by the set of boundary conditions,[1]

$$\psi(x,Z) = \Psi(x) \qquad \text{jet influx} \tag{5a}$$

$$\psi(x,0) = 0 \qquad \text{surface plane} \tag{5b}$$

$$\psi(0,z) = 0 \qquad \text{jet axis} \tag{5c}$$

$$\psi(X,z) = \Psi(\sqrt{2Xz}) \qquad \text{jet efflux} \tag{5d}$$

where X and Z are sufficiently removed from the origin that further movement leaves the solutions unchanged.

The jet profiles for this study are given in Table 1 and are such that for $x_m \to 0$ the defect vanishes and the fully developed profiles used by Rubel[1] are recovered. The jet momentum J is

$$\left(\frac{J}{2\pi}\right)_{x\to\infty} = x_m^2\left(\frac{\delta w^2}{10} - \frac{\delta w}{3} + \frac{1}{2}\right) + \frac{5\pi}{32}\frac{x_m}{\sqrt{c_m}} + \frac{1}{6c_m}$$

$$c_m \equiv \frac{(\sqrt{2}-1)}{(1-x_m)^2} \tag{6}$$

and it is useful for comparison with the integrated surface pressure force. That is,

$$\left(\frac{J}{2\pi}\right)_{\infty} = \frac{1}{2}\int_0^{\infty} p(x,0)x\,dx \tag{7}$$

where the pressure p is scaled by the maximum dynamic pressure of the jet. The pressure field can be found by integration of the momentum equation, so that

$$p(x,z) = w^2(\Psi) - u^2(x,z) - w^2(x,z); \quad \psi \geq 0 \tag{8a}$$

where $w^2(\Psi)$ is the total pressure on $\psi(x,z)$ and, under the conditions of Eq. (4),

$$p(x,z) = w^2(0) - u^2(x,z) - w^2(x,z) + 2\Omega(0)\psi(x,z); \quad \psi \leq 0 \tag{8b}$$

Numerical solution of Eq. (1) for the velocity profiles of Table 1 is made difficult because the vorticity function is related implicitly to the stream function. However, if a parametric function g is defined in terms of the influx profiles by

$$\psi(g) \equiv \Psi(x^2); \quad g \geq 0 \tag{9}$$

then both the stream function and vorticity function are explicitly related to g and the value of g is also "frozen" on streamlines. Within a recirculation zone (i.e., $g<0$) an explicit relationship must be devised which matches conditions on the dividing streamline, viz.

$$\psi = 0, \quad \frac{\partial\psi}{\partial g} = \frac{1-\delta w}{2}, \quad \frac{\partial^2\psi}{\partial g^2} = \frac{\delta w}{x_m^2}; \quad g = 0$$

The form chosen here is

$$\psi(g) = \frac{(1-\delta w)}{2}g + \frac{\delta w}{2x_m^2}g^2 + \frac{N\delta w^2}{6x_m^4(1-\delta w)}g^3; \quad g \leq 0 \tag{10}$$

where the third term is added to ensure that $\psi(g)$ is single valued (i.e., for $N>1$). Otherwise, the value of N has no effect whatever on the solution. Recasting Eqs. (1) and (5) in the variable g yields

$$\frac{\partial^2 g}{\partial z^2} + \frac{\partial^2 g}{\partial x^2} - \frac{1}{x}\frac{\partial g}{\partial x} + \left[\left(\frac{\partial g}{\partial x}\right)^2 + \left(\frac{\partial g}{\partial z}\right)^2\right]\frac{\partial^2\psi/\partial g^2}{\partial\psi/\partial g} - \frac{x^2\Omega(g)}{\partial\psi/\partial g} = 0 \tag{11}$$

$$g(x,Z) = x^2 \qquad \text{jet influx} \tag{12a}$$

$$g(x,0) = 0 \qquad \text{surface plane} \tag{12b}$$

$$g(0,z) = 0 \qquad \text{jet axis} \tag{12c}$$

$$g(X,z) = 2Xz \qquad \text{jet efflux} \tag{12d}$$

Two final transformations complete the formulation. New independent variables $(\bar{x},\bar{z})$ are defined by

$$x = \bar{x}, \qquad z = \bar{z}^2/2X \tag{13}$$

in order to resolve more finely the region near the surface plane. This allows better definition for the numerical description of the surface pressure [i.e., Eq. (8a)] and for the detection of recirculation zones. Also, in order that the dependent variable be scaled by unity a new dependent variable is defined:

$$f = \arctan(g) \tag{14}$$

Table 1 Jet profiles

	$0 \leq x \leq x_m$	$x \geq x_m$
Stream function $\Psi(x)$	$\frac{x^2}{2}\left[1-\delta w+\delta w\frac{x^2}{x_m^2}\left(1-\frac{1}{3}\frac{x^2}{x_m^2}\right)\right]$	$\Psi(x_m) + \frac{x(x-x_m)}{2[1+c_m(x-x_m)^2]} + \frac{x_m}{2\sqrt{c_m}}\arctan[\sqrt{c_m}(x-x_m)]$
Velocity $-w(x)$	$1-\delta w+2\delta w\frac{x^2}{x_m^2}\left(1-\frac{1}{2}\frac{x^2}{x_m^2}\right)$	$[1+c_m(x-x_m)^2]^{-2}$
Vorticity function $\Omega(x)$	$4\frac{\delta w}{x_m^2}\left(1-\frac{x^2}{x_m^2}\right)$	$\frac{-4c_m\left(1-\frac{x_m}{x}\right)}{[1+c_m(x-x_m)^2]^3}; \quad c_m = \frac{\sqrt{2}-1}{(1-x_m)^2}$

The system of governing equations now takes the form

$$\frac{\partial^2 f}{\partial \bar{z}^2} - \frac{1}{\bar{z}}\frac{\partial f}{\partial \bar{z}} + \frac{\bar{z}^2}{\bar{X}^2}\left(\frac{\partial^2 f}{\partial \bar{x}^2} - \frac{1}{\bar{x}}\frac{\partial f}{\partial \bar{x}}\right) + \left[2g + \frac{\partial^2\psi/\partial g^2}{\partial\psi/\partial g}(1+g^2)\right]\left[\left(\frac{\partial f}{\partial \bar{z}}\right)^2 + \frac{\bar{z}^2}{\bar{X}^2}\left(\frac{\partial f}{\partial \bar{x}}\right)^2\right] = \frac{\bar{z}^2}{\bar{X}^2}\frac{\bar{x}^2}{(1+g^2)}\frac{\Omega(g)}{\partial\psi/\partial g}, \quad g=\tan f \tag{15}$$

$$f(\bar{x},\bar{Z}) = \arctan(\bar{x}^2) \qquad \text{jet influx} \tag{16a}$$

$$f(\bar{x},0) = 0 \qquad \text{surface plane} \tag{16b}$$

$$f(0,\bar{z}) = 0 \qquad \text{jet axis} \tag{16c}$$

$$f(\bar{X},\bar{z}) = \arctan(\bar{z}^2) \qquad \text{jet efflux} \tag{16d}$$

Computational Results

The partial differential equation, Eq. (15), subject to its Dirichlet boundary conditions [Eq. (16)] can be solved numerically by rather standard techniques. Here, a uniform grid is applied in each coordinate direction (e.g., Fig. 2) so that the computational boundaries are aligned with $\bar{x}=0,\bar{X}$ and $\bar{z}=0,\bar{Z}$. The derivatives of $f(\bar{x},\bar{z})$ are represented by central differences and the resulting set of algebraic equations are solved by SLOR using a tridiagonal solver along $\bar{x}=$ const lines and sweeping from $\bar{x}=0$ to $\bar{x}=\bar{X}$. Experience has shown[1,11] that $X=5$, $Z=2.5$ (i.e., $\bar{X}=5$, $\bar{Z}=5$) places the boundaries appropriately distant from the origin for computations of this type. Unless otherwise specified, these values have been used on a (51×401) grid to generate the present results. All solutions are converged with maximum residuals less than 10^{-6}, which generally is a 10^{-9} reduction with respect to the initial residual.

The code was verified by calculating a fully developed profile case ($x_m=0$, $\delta w=0$) and a case representative of a potential jet ($x_m=0.8$, $\delta w=0$, $X=4$, $Z=2$, 41×401 grid). Comparison of ground plane pressure distributions, normalized by the stagnation pressure p_s with the data of Giralt et al.[11] and Brady and Ludwig,[12] show excellent agreement (Fig. 3). The pressures were computed from Eqs. (8a) and (12) by using the surface value of vorticity in a Taylor expansion for the stream function over a single mesh width. The fully developed solution is also in agreement with previous numerical work[1]; the "potential" solution, by this approach, is shown for the first time. These computations, and all others presented here, satisfy the integrated surface pressure force relationship, Eq. (7), with error less than 2%.

A series of cases with $x_m=0.35$ and various degrees of velocity defect were computed, and the appearance of stagnation bubbles was established. The development of the recirculation zones is best shown with streamline plots (Fig. 4). When the velocity defect is zero (Fig. 4a), streamlines take on the usual impact zone appearance. Their smooth, nearly parallel nature at the influx and efflux boundaries are an indication that the computational domain is adequate. When the defect is increased to $\delta w=0.10$ (Fig. 4b), a recirculation zone appears in the stagnation region which acts to displace the neighboring streamlines. Further increase in the defect to $\delta w=0.16$ (Fig. 4c), shows considerable growth of the bubble and a marked change in the shape of adjacent streamlines. All attempts at calculations with larger defects (e.g., $\delta w=0.17$, $x_m=0.35$) met with failure.

The range of computation was extended to encompass cases where the jet velocity peak moved closer to, as well as further from, the jet axis. For $0.25\le x_m\le 0.55$, a similar behavior was noted (Fig. 5). There is a small velocity defect regime where the impingement structure is of the usual type. Increases in the defect produce stagnation bubbles which grow with the defect until a maximum defect value is reached beyond which no solution is found (i.e., the iterative procedure diverges).

This result was generated using a family of velocity profiles (Table 1) with axis vorticity function constrained by $\Omega(0)x_m^2/\delta w=4$. Computer experiments with other velocity profiles revealed that the classification of numerical results (Fig. 5) is qualitatively independent of the value of the axis vorticity function. However, as the limit $\Omega(0)x_m^2/\delta w=0$ is approached, the $(\delta w, x_m)$ domain where recirculation zone solutions are detectable vanishes and the numerical results are classified by either "no solution found" or "no recirculation zone." This observation is consistent with the axisymmetric statement of the Batchelor condition (Eq. 4). At the jet axis, symmetry dictates that the vorticity ω is always zero whereas the vorticity function, $\Omega(0)$, vanishes only when the incoming velocity profile has no centerline curvature [Eq. (3), $x\to0$]. If a recirculation zone is to be found under these circumstances, then it must be a region of zero vorticity function and, hence, be vorticity-free. Since this is not possible, no stagnation bubble can exist when $\Omega(0)=0$.

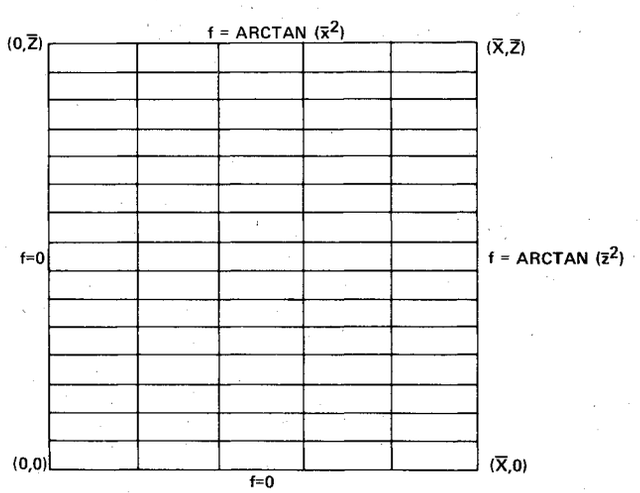

Fig. 2 Computational domain and boundary conditions.

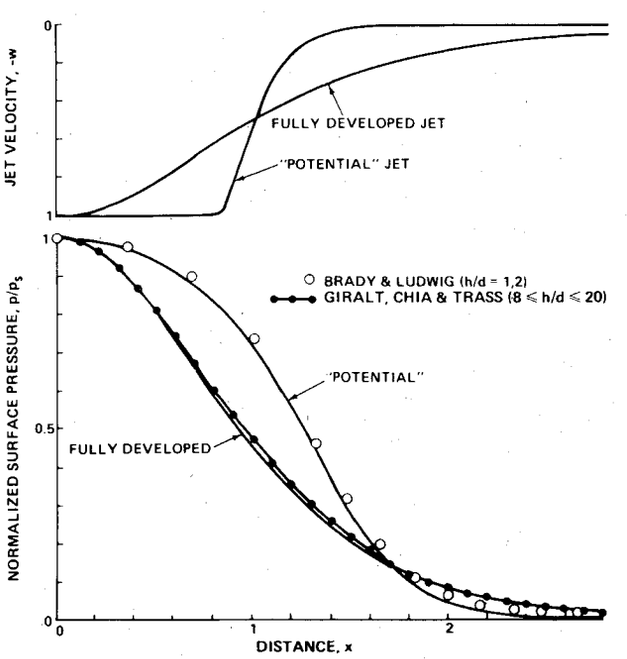

Fig. 3 Surface plane pressure distribution, computation vs experiment.

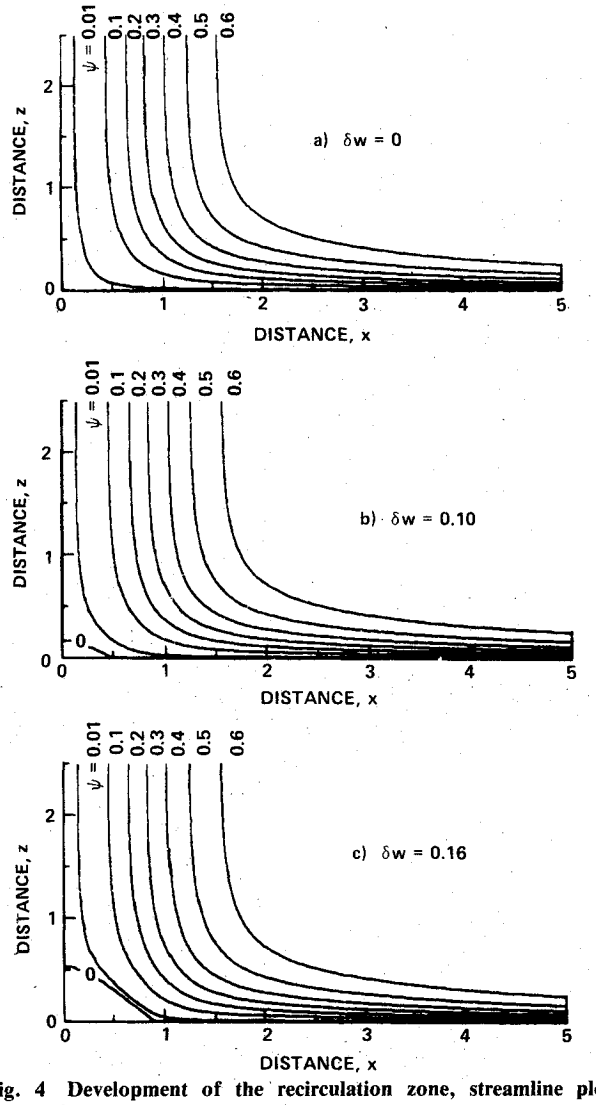

Fig. 4 Development of the recirculation zone, streamline plots ($x_m = 0.35$).

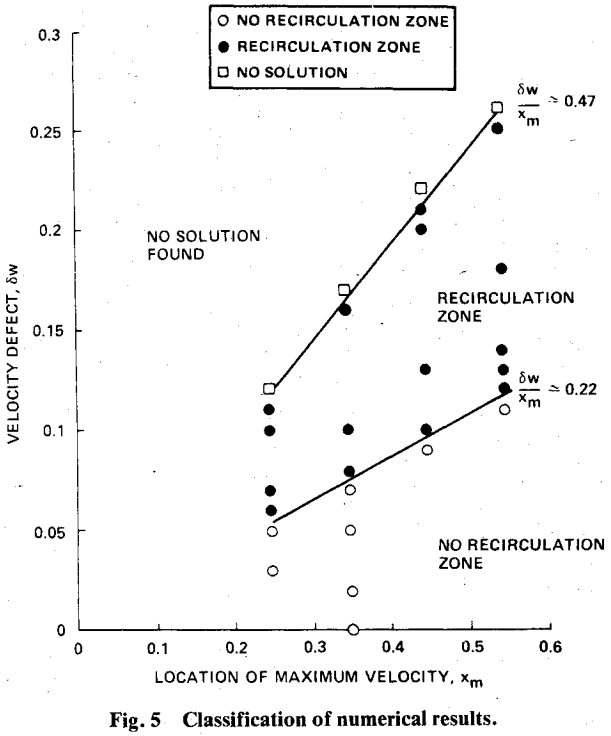

Fig. 5 Classification of numerical results.

Table 2 Jet core profiles—zero axis vorticity function ($x \le x_m$)

Stream function $\Psi(x)$	$x^2\left[\frac{(1-\delta w)}{2}+\frac{4}{5}\delta w\frac{x^3}{x_m^3}\left(1-\frac{5}{8}\frac{x}{x_m}\right)\right]$
Velocity $-w(x)$	$1-\delta w+4\delta w\frac{x^3}{x_m^3}\left(1-\frac{3}{4}\frac{x}{x_m}\right)$
Vorticity function $\Omega(x)$	$12\frac{\delta w}{x_m^2}\frac{x}{x_m}\left(1-\frac{x}{x_m}\right)$

To illustrate this point, core (i.e., $x<x_m$) profiles with zero axis vorticity function were chosen (Table 2) and the cases ($x_m = 0.35$; $\delta w = 0.1$, 0.16) were recomputed. In place of a stagnation bubble, the velocity defect causes a sizable region of low speed fluid near the stagnation point (Fig. 6). Comparison of the surface pressure distributions ($x_m = 0.35$; $\Omega(0) = 0$, $\Omega(0) \neq 0$) shows that the flow structure in the stagnation region is quite sensitive to the velocity defect profile and that the extent of the high pressure region about the stagnation point is determined by the magnitude of the defect (Fig. 7). Also apparent here is the 15% drop in pressure that results from the large reversed flow region at $\delta w = 0.16$, $\Omega(0) \neq 0$.

It should be noted that the character of these pressure distributions bears a resemblance to those observed in the context of supersonic jet impingement[5] while the computed stagnation bubble shapes are consistent with the overall features described by Kalghatgi and Hunt.[4] Perhaps the inviscid total pressure defect mechanism has some relevance to the occurrence of stagnation bubbles in the underexpanded jet impact problem.

Local Recirculation Zone Solution

If Eq. (1) is rewritten in spherical, polar coordinates then

$$\frac{\partial^2\psi}{\partial r^2}+\frac{\sin\theta}{r^2}\frac{\partial}{\partial\theta}\left(\frac{1}{\sin\theta}\frac{\partial\psi}{\partial\theta}\right)=\Omega(\psi)r^2\sin^2\theta \tag{17}$$

where $x = r\sin\theta$, $z = r\cos\theta$. For the constant vorticity function regions that have been discussed here, Eq. (17) has a particular solution[9]

$$\psi_p = (\Omega/10)r^4\sin^2\theta \tag{18}$$

where $\Omega(\psi) \equiv \Omega$. The homogeneous solution can be deduced from the stream function relationship to the zonal harmonic potential result,[13] so that the solution to Eq. (17) has the form

$$\psi = \sin^2\theta\left[\frac{\Omega}{10}r^4+\sum_{k=1}^{n}A_k r^{k+1}P_k'(\cos\theta)\right] \tag{19}$$

Here, $P_k(\cos\theta)$ is the Legendre polynomial of order k. This solution is easily verified via substitution of Eq. (19) into Eq. (17), which produces the differential equation that defines the Legendre function.

Hill's spherical vortex[8,9] is represented by Eq. (19) for $A_1 = -\Omega/10$, $A_k = 0$, $k \neq 1$. The boundary conditions required here, viz.

$$\psi = 0 \quad \text{at} \quad \theta = 0,\ \pi/2 \tag{20}$$

are not satisfied by the Hill solution and, in fact, $A_1 = 0$. The condition at $\theta = 0$ is always satisfied by Eq. (19). In order to sustain a recirculation bubble the summation of Eq. (19) must span at least three terms. Furthermore, for a local solution

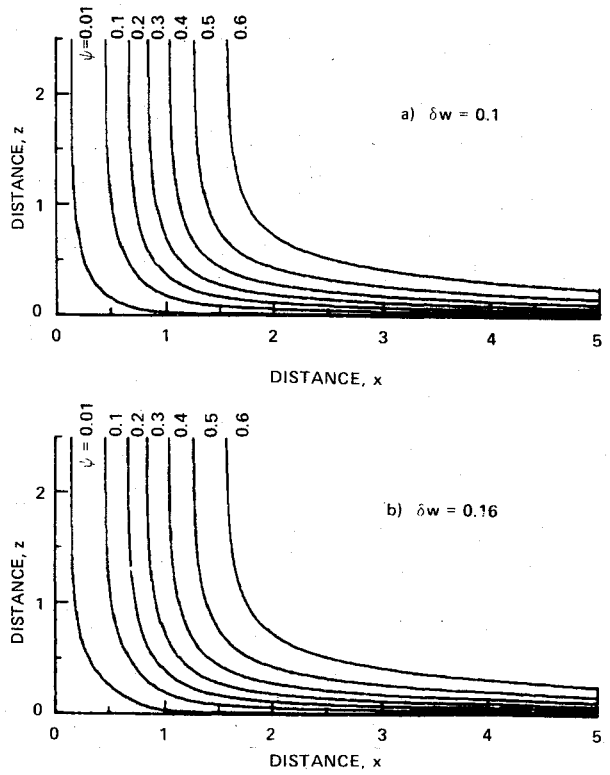

Fig. 6 Flow structure when centerline vorticity function is zero, $\Omega(0)=0$ streamline plots ($x_m=0.35$).

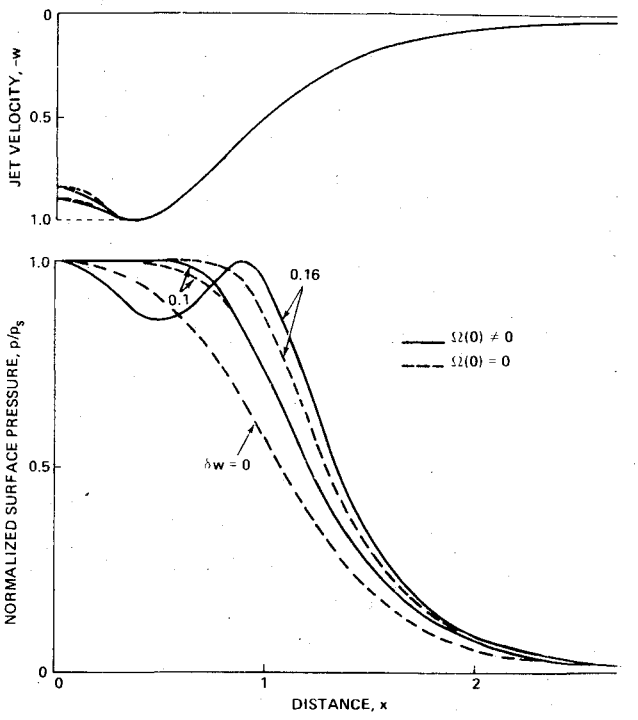

Fig. 7 Effect of velocity defect on surface plane pressure distribution.

about the origin, terms of lowest order powers in r are expected to dominate. The coefficient A_3 is determined to satisfy Eq. (20),

$$A_3=-\frac{\Omega/10}{P_3'[\cos(\pi/2)]}=\frac{\Omega}{15} \tag{21}$$

reducing Eq. (19) to

$$\psi=\tfrac{1}{2}r^3\sin^2\theta\cos\theta\,[6A_2+\Omega r\cos\theta+5A_4r^2(7\cos^2\theta-3)] \tag{22}$$

The condition that $\psi=0$ on the dividing streamline is manifested by the vanishing of the square bracket term in Eq. (22). If this constraint is imposed at the axis and surface intercepts, that is $x=x_0$, $z=z_0$ (Fig. 1) then

$$A_2=-\frac{\Omega z_0}{6(1+B)}, \qquad A_4=-\frac{\Omega z_0}{15x_0^2(1+B)}$$

where

$$B=\frac{4}{3}\left(\frac{z_0}{x_0}\right)^2$$

Recasting Eq. (22) into the cylindrical coordinate variables yields the result

$$\psi=-\frac{\Omega}{2}\frac{x_0^2z_0^2}{1+B}\,[(1-\tilde{z})(1-B\tilde{z})-\tilde{x}^2]\tilde{x}^2\tilde{z} \tag{23}$$

where the definitions $\tilde{x}=x/x_0$, $\tilde{z}=z/z_0$ are convenient.

Much of the structure of the axisymmetric stagnation bubble is evident from Eq. (23). The solution is well behaved, in contrast to the two-dimensional normal impingement case which exhibits an $r^2\ln r$ singularity.[14] The definition of the dividing streamline is established as a function of the geometric parameter B (Fig. 8) and B is limited to values between zero and unity. Thus, the greatest aspect ratio that

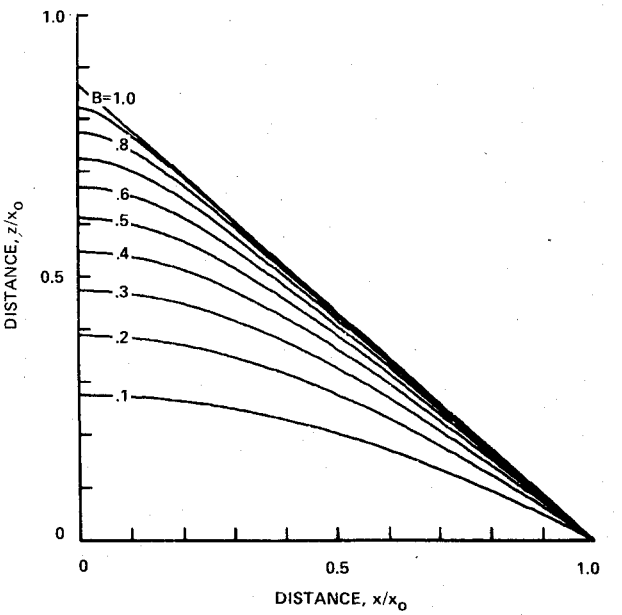

Fig. 8 Dividing streamline solutions for axisymmetric recirculation zone.

this model allows is

$$(z_0/x_0)_{\max}=\tfrac{1}{2}\sqrt{3} \tag{24}$$

Along the dividing streamline the stagnation point at the jet axis is axisymmetric in nature, whereas the off-axis stagnation point is two-dimensional. Except for the limiting $B=1$ case, the dividing streamline is normal to the jet axis and inclined at angle β,

$$\beta=\arctan[\sqrt{3B}/(1+B)] \tag{25}$$

at the off-axis position. The largest inclination is for $B=1$, where the dividing streamline is given by $\tilde{x}=1-\tilde{z}$ and $\beta=\arctan(\tfrac{1}{2}\sqrt{3})$.

Table 3 Recirculation zone results

					Numerical			Analytical	
x_m	δw	x_0	z_0	B	$2\Omega\psi_{min}$	u_{min}	ψ_{min}	u_{min}	ψ_{min}
0.25	0.11	0.688	0.393	0.435	−0.0704	−0.252	−0.00486	−0.255	−0.00500
0.35	0.16	0.890	0.533	0.478	−0.1135	−0.323	−0.01094	−0.323	−0.01086
0.45	0.21	1.126	0.723	0.550	−0.1923	−0.426	−0.0242	−0.419	−0.0232
0.55	0.25	1.236	0.798	0.556	−0.1779	−0.411	−0.0282	−0.403	−0.0269
0.70	0.30	1.319	0.831	0.530	−0.1244	−0.336	−0.0257	−0.338	−0.0254
0.75	0.32	1.395	0.903	0.558	−0.1370	−0.360	−0.0314	−0.354	−0.0301

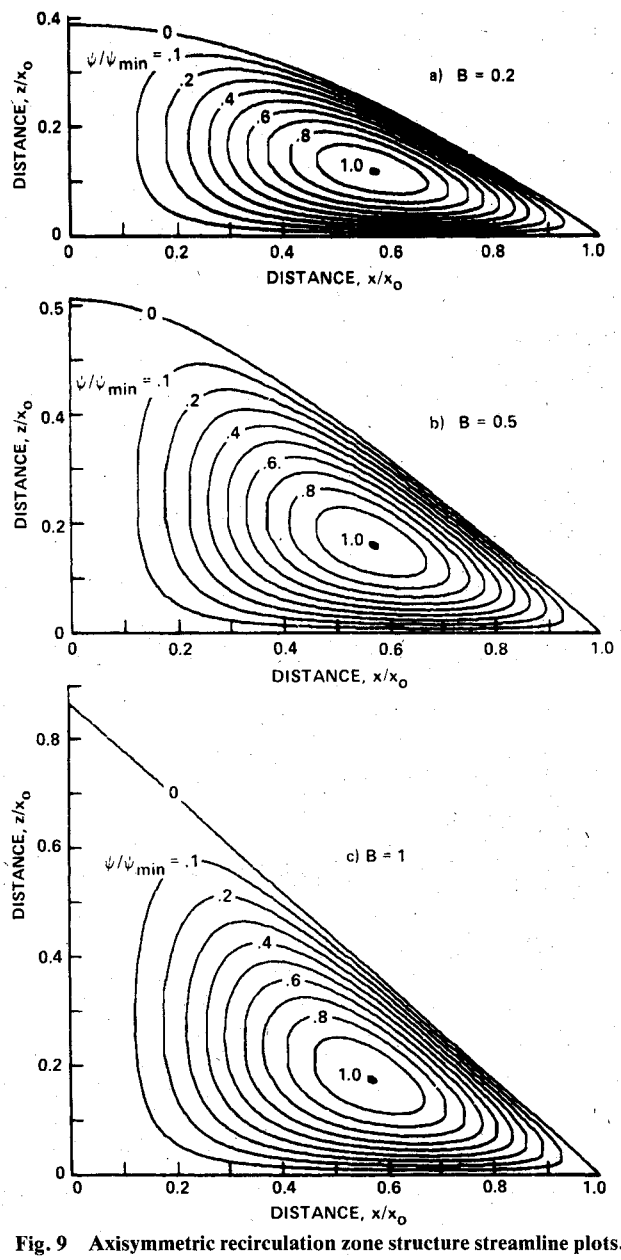

Fig. 9 Axisymmetric recirculation zone structure streamline plots.

Streamline plots (Fig. 9) reveal flow patterns that are independent of the value of B. It is easily derived that the minimum stream function ψ_{min} occurs at

$$\tilde{z}_{min} = \frac{3}{10}\,\frac{(1+B)}{B}\left[1-\left(1-\frac{20B}{9(1+B)^2}\right)^{1/2}\right] \tag{26a}$$

$$\tilde{x}^2_{min} = \frac{2}{5}\left[1-\frac{1}{2}(1+B)\,\tilde{z}_{min}\right] \tag{26b}$$

and has the value

$$\psi_{min} = -\frac{\Omega x_0^2 z_0^2}{2(1+B)}\,\tilde{x}^4_{min}\tilde{z}_{min} \tag{27}$$

So, the location of the minimum varies little [viz., $1/3 \geq \tilde{z}_{min} \geq 1/5$, $1/\sqrt{3} \geq \tilde{x}_{min} \geq (2/5)\sqrt{2}$] and, in fact, $\tilde{x}_{min}$ is practically independent of parameter B (Fig. 9). The magnitude of ψ_{min} is useful for indicating vortex strength in terms of the total pressure difference within the bubble via Eq. (8b). The greatest negative velocity on the surface, u_{min}, is

$$u_{min} = \frac{\Omega x_0 z_0}{3\sqrt{3}(1+B)} \quad \text{at} \quad \tilde{x} = \frac{1}{\sqrt{3}}$$

and the magnitude of the peak velocity along the dividing streamline can be shown to be within +4% or −2% of the magnitude of u_{min}.

Features of the recirculation zone obtained from the overall numerical calculations are compared with their local analytical solution counterparts for selected cases (Table 3). The values of x_0 and z_0, taken from the overall solutions, yield a common range for parameter B (i.e., $B \approx 0.5$) although varying vortex strengths (i.e., $2\Omega\psi_{min}$) are represented. Maximum discrepancies of only 4% in ψ_{min} and 2% in u_{min} are noted and this agreement confirms the relationship between the local solution, Eq. (23), and the overall impingement result.

Conclusions

The normal impingement of axisymmetric jets with velocity deficient cores is studied here. From a theoretical/numerical analysis of the inviscid, incompressible impact region the following conclusions are reached:

1) The numerical results fall into three categories: a) a small defect regime where no stagnation bubble is observed, b) a moderate defect regime where recirculation zones appear and grow with the defect, c) a large defect regime where no solutions have been attained.

2) Numerical experiments indicate that the appearance of stagnation bubbles is sensitive to the axis vorticity function. Nevertheless, the extent of the low velocity stagnation region, even with no bubble, is dependent upon the velocity defect magnitude.

3) A local stagnation bubble solution, of the Hill's spherical vortex[8,9] genre, is derived. It is demonstrated that this result is consistent with finite difference impingement computations.

References

[1] Rubel, A., "Computations of Jet Impingement on a Flat Surface," *AIAA Journal*, Vol. 18, 1980, pp. 168-175.

[2] Hill, W. G. Jr. and Jenkins, R. C., "Ground Impingement of a Fan Jet Exhaust Plume," Grumman Research Dept., Bethpage, N. Y., RM-653, 1978.

[3] Donaldson, C. duP. and Snedeker, R. S., "A Study of Free Jet Impingement. Part 1, Mean Properties of Free and Impinging Jets," *Journal of Fluid Mechanics*, Vol. 45, 1971, pp. 281-319.

[4]Kalghatgi, G. T. and Hunt, B. L., "The Occurrence of Stagnation Bubbles in Supersonic Jet Impingement Flows," *Aeronautical Quarterly,* Vol. 27, 1976, pp. 169-185.

[5]Lamont, P. J. and Hunt, B. L., "The Impingement of Underexpanded, Axisymmetric Jets on Perpendicular and Inclined Flat Plates," *Journal of Fluid Mechanics,* Vol. 100, 1980, pp. 471-511.

[6]Bossel, H. H., "Vortex Breakdown Flowfield," *Physics of Fluids,* Vol. 12, 1969, pp. 498-508.

[7]Hafez, M. and Lovell, D., "Numerical Solution of Transonic Stream Function Equations," *Proceedings of AIAA 5th Computational Fluid Dynamics Conference,* Palo Alto, Calif., June 1981, pp. 364-372.

[8]Batchelor, G. K., *An Introduction to Fluid Dynamics,* Cambridge University Press, Cambridge, England, 1967, pp. 525-526.

[9]Milne-Thomson, L. M., *Theoretical Hydrodynamics,* 4th ed., The Macmillan Co., New York, N. Y., 1969, pp. 554-555.

[10]Batchelor, G. K., "On Steady Laminar Flow with Closed Streamlines at Large Reynolds Number," *Journal of Fluid Mechanics,* Vol. 1, 1956, pp. 177-190.

[11]Giralt, F., Chia, C. J., and Trass, O., "Characterization of the Impingement Region in an Axisymmetric Turbulent Jet," *Industrial and Engineering Chemistry Fundamentals,* Vol. 16, 1977, pp. 21-28.

[12]Brady, W. G. and Ludwig, G., "Theoretical and Experimental Studies of Impinging Uniform Jets," IAS Paper 63-29, IAS 31st Annual Meeting, New York, N. Y., Jan. 1963.

[13]Morse, P. M. and Feshback, H., *Methods of Theoretical Physics,* McGraw-Hill Book Co., Inc., New York, N. Y., 1953, pp. 1264-1266.

[14]Fraenkel, L. E., "On Corner Eddies in Plane Inviscid Shear Flow," *Journal of Fluid Mechanics,* Vol. 11, 1961, pp. 400-406.